Title

THE EFFECTS OF A FINITE NUMBER OF PROJECTION ANGLES and FINITE LATERAL SAMPLING OF PROJECTIONS ON THE PROPAGATION OF STATISTICAL ERRORS IN TRANSVERSE SECTION RECONSTRUCTION

Author

Huesman, R.H.

Publication Date

1976-07-01

Submitted to Physics in Medicine and Biology

LBL-4773
Preprint

THE EFFECTS OF A FINITE NUMBER OF PROJECTION ANGLES AND FINITE LATERAL SAMPLING OF PROJECTIONS ON THE PROPAGATION OF STATISTICAL ERRORS IN TRANSVERSE SECTION RECONSTRUCTION

R. H. Huesman

DONNER LABORATORY

July 1976

Prepared for the U. S. Energy Research and Development Administration under Contract W-7405-ENG-48

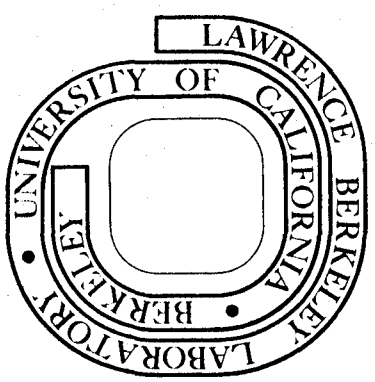

DISCLAIMER

LBL-4773

The Effects of a Finite Number of Projection Angles and Finite Lateral Sampling of Projections on the Propagation of Statistical Errors in Transverse Section Reconstruction

R. H. Huesman, Ph.D

Lawrence Berkeley Laboratory
University of California
Berkeley, California

July 1976

The Effects of a Finite Number of Projection Angles and Finite Lateral Sampling of Projections on the Propagation of Statistical Errors in Transverse Section Reconstruction

R. H. Huesman, Ph.D.

Lawrence Berkeley Laboratory

University of California

Berkeley, California

July 1976

ABSTRACT. The dependence of noise amplification on the number of projection angles and on the lateral sampling interval of projections is presented. It is shown that about 1.5 D/d angles and a sampling interval of about .5d are required in order that the data be efficiently utilized. (D is the linear dimension of the reconstruction region and d is the linear dimension of the cells into which the reconstruction region is subdivided.) Values for noise amplification are given for various combinations of projection angles and lateral sampling intervals.

1. Introduction

Techniques for reconstruction of the 3-dimensional distribution of density in an object from projections at multiple angles have received extensive investigation and review, particularly for x-ray transmission (Gordon and Herman 1973) and photon emission from radioisotopes (Budinger and Gullberg 1974). Previous analyses of the expected uncertainty in a reconstruction due to statistical fluctuations in the measurements have been performed for several reconstruction algorithms under the assumption of adequate number of projections: iterative relaxation (Goitein 1972), convolution or filtering of the projections with subsequent backprojection (Shepp and Logan 1974, Barrett et. al. 1975, Chesler 1975, Tanaka and Iinuma 1975), Radon inversion (Friedman, Beattie and Laughlin, 1974) and convolution or filtering of the backprojection (Huesman 1975). The present work gives the dependence of noise amplification on the number of projection angles and on the sampling interval of projections. The analysis is applied to the noise propagation for iterative techniques in the limit that the least squares solution is reached. Errors or artifacts in the reconstruction unrelated to statistical fluctuations in the projection data are not considered here.

This analysis is carried out using a circular reconstruction region of diameter D which is subdivided into small square cells of dimension d x d. The area to be reconstructed consists of $\nu \simeq (\pi/4)\ (D/d)^2$ cells, each of which is assumed to contain uniform density. The data consist of a collection of line integrals of the density over n coplanar paths through the transverse section. The paths traverse the reconstruction region at n_z regularly spaced intervals and at n_θ regularly spaced angles such that $n = n_\theta n_z$. The geometry of the reconstruction region and an example of the paths for line integrals at one angle, θ, are shown in fig. 1. For the model chosen (uniform density in each cell) the relationship between the line integral I_i and the density, ρ_j in the j^{th} cell is,

$$I_i = \sum_{j=1}^{\nu} \ell_{ij}\ \rho_j \qquad (1)$$

where ℓ_{ij} is the line length of the i^{th} path through the j^{th} cell, as shown in the inset of fig. 1. (ℓ_{ij} is zero if the i^{th} path does not intersect the j^{th} cell.) For finite width paths, ℓ_{ij} should be replaced by the area common to the i^{th} path and the j^{th} cell divided by the path width.

2. Reconstruction and Error Analysis

The backprojection (simple superposition image) B_k, for the k^{th} cell is proportional to the line integral times the line length through that cell summed over the n paths.

$$B_k = \frac{D}{nd^3} \sum_{i=1}^{n} I_i \ell_{ik} \tag{2}$$

The choice of the normalization factor $D/(nd^3)$ is explained below.

By substitution of eqn (1) into eqn (2), the backprojection can be written in terms of the density as,

$$B_k = \frac{D}{nd^3} \sum_{i=1}^{n} \sum_{j=1}^{\nu} \ell_{ik} \ell_{ij} \rho_j \tag{3}$$

Defining the matrix M by the expression,

$$M_{kj} = \frac{D}{nd^3} \sum_{i=1}^{n} \ell_{ik} \ell_{ij} \tag{4}$$

and substituting into eqn (3), gives,

$$B_k = \sum_{j=1}^{\nu} M_{kj} \rho_j \tag{5}$$

so that the backprojection vector is just the density vector multiplied by the matrix M. A diagonal element of M is given by.

$$M_{jj} = \frac{D}{nd^3} \sum_{i=1}^{n} \ell_{ij}^2 \tag{6}$$

but the fraction of line lengths which are non-zero is about d/D (only about nd/D of the line integrals intersect the j^{th} cell) and when non-zero, ℓ_{ij} is about equal to d (the linear dimension of a cell) so that

$$M_{jj} \simeq \frac{D}{nd^3} \frac{nd}{D} d^2 = 1 \tag{7}$$

Thus the normalization factor $D/(nd^3)$ makes the matrix M roughly independent of the number of line integrals and the geometry of the reconstruction region. In the Appendix it is shown that in the limit of large n_θ and n_z, M_{kj} approaches $(d/\pi) < r_{kj}^{-1} >$, where $< r_{kj}^{-1} >$ is the average inverse distance between points in the j^{th} and k^{th} cells; and that furthermore $(d/\pi) < r_{jj}^{-1} > = .95$.

In order to investigate the uncertainty in the reconstruction, the density vector is expressed in terms of the inverse of the matrix M as,

$$\rho_j = \sum_{k=1}^{\nu} M_{jk}^{-1} B_k = \sum_{k=1}^{\nu} M_{jk}^{-1} \frac{D}{nd^3} \sum_{i=1}^{n} I_i \ell_{ik} = \frac{D}{nd^3} \sum_{i=1}^{n} I_i \sum_{k=1}^{\nu} M_{jk}^{-1} \ell_{ik} \tag{8}$$

Since the measurements of different line integrals are statistically independent, the statistical rms error of ρ_j is the sum of the rms errors of the contributions from each I_i added in quadrature,

$$\begin{aligned} \sigma^2(\rho_j) &= \left(\frac{D}{nd^3}\right)^2 \sum_{i=1}^{n} \sigma^2(I_i) \left(\sum_{k=1}^{\nu} M_{jk}^{-1} \ell_{ik} \right)^2 \\ &= \left(\frac{D}{nd^3}\right)^2 \sum_{i=1}^{n} \sigma^2(I_i) \sum_{k=1}^{\nu} \sum_{m=1}^{\nu} M_{jk}^{-1} M_{jm}^{-1} \ell_{ik} \ell_{im} \end{aligned} \tag{9}$$

where $\sigma(\rho_j)$ and $\sigma(I_i)$ are the rms errors of ρ_j and I_i respectively. If the rms errors of all I_i are equal to σ_I,

$$\sigma^2(\rho_j) = \left(\frac{D\sigma_I}{nd^3}\right)^2 \sum_{k=1}^{\nu} \sum_{m=1}^{\nu} M_{jk}^{-1} M_{jm}^{-1} \sum_{i=1}^{n} \ell_{ik} \ell_{im} \tag{10}$$

and substitution from eqn (4) gives,

$$\sigma^2(\rho_j) = \frac{D\sigma_I^2}{nd^3} \sum_{k=1}^{\nu} \sum_{m=1}^{\nu} M_{jk}^{-1} M_{jm}^{-1} M_{km} = \frac{D\sigma_I^2}{nd^3} M_{jj}^{-1} \tag{11}$$

Eqn (8) is the standard unweighted least squares solution of eqn (1) with $D/(nd^3)$ factored out to make the results of the error analysis more transparent. Just as the matrix M is independent of the number of line integrals, so are the diagonal elements of its inverse in the limit of large n_θ and n_z (as will be shown in the next section). The derivation of eqn (11) assumes that the uncertainties of all measured line integrals are equal, but practical estimates can be made when this assumption is not true.

3. Infinite Number of Data Points (Line Integrals)

As mentioned above, when n_θ and n_z are sufficiently large M_{kj} depends only on the relative coordinates of the j^{th} and k^{th} cells and therefore multiplication by the matrix M becomes a discrete convolution with the function $(d/\pi) < r^{-1} >$. The diagonal elements of the matrix M are equal, and the off diagonal elements decrease proportional to the reciprocal of the distance between cells. That is, M_{jk} is proportional to the reciprocal of the distance between the k^{th} and j^{th} cells. Using values for M_{jk} given by eqn (A14) of the Appendix, the matrix M has been inverted for D/d (the number of cells across the circular region) equal to 8, 16, and 32. In these cases, for all cells except those at the very edge of the reconstruction region, $M_{jj}^{-1} = 1.5917 \pm .001$. Since the value of M_{jj}^{-1} remains so stable over this range, it is assumed that $M_{jj}^{-1} = 1.59$ is reliable for arbitrarily large values of D/d.

Setting M_{jj}^{-1} equal to 1.59 in eqn (11) gives,

$$\sigma^2(\rho_j) = \frac{1.59\ D}{nd^3} \sigma_I^2 \tag{12}$$

or

$$\sigma_\rho = \sqrt{\frac{1.59\ D}{nd^3}}\ \sigma_I \tag{13}$$

where σ_ρ is the rms error of all reconstructed cell densities, since there is no j-dependence on the right-hand side of eqn (12).

The average value of the line integrals I_i for the circular reconstruction region is found from eqn (1) to be,

$$\langle I \rangle = \frac{\pi D \langle \rho \rangle}{4} \tag{14}$$

and division of eqn (13) by eqn (14) gives,

$$\frac{\sigma_\rho}{\langle \rho \rangle} = .99 \sqrt{\frac{D^3}{nd^3}} \frac{\sigma_I}{\langle I \rangle} \simeq \sqrt{\frac{D^3}{nd^3}} \frac{\sigma_I}{\langle I \rangle} \tag{15}$$

where $\langle \rho \rangle$ is the average value of the density within the reconstruction region.

Eqn (13) was previously derived under the same assumptions of large n_θ and n_z and the same model of a reconstruction region partitioned into square cells of uniform density (Huesman 1975). Two methods of reconstruction were shown to arrive at this result: convolution of the backprojection and filtering of the backprojection. In both cases the convolution function (or filter function) was chosen to give the best possible resolution. When high frequency components are suppressed to reduce noise the resolution is degraded. Eqn (13) is applicable to any of the iterative techniques which converge to the least squares solution of eqn (1) under the assumptions of equal uncertainties for the measurements of the line integrals as well as large n_θ and n_z. Eqn (15) is essentially the same as the estimate made for the iterative relaxation technique by Goitein (1972).

Results similar to eqns (13) and (15) have been derived for the methods of convolution and filtering of the projections with subsequent backprojection (Shepp and Logan 1974, Barrett et. al. 1975, Chesler 1975, Tanaka and Iinuma 1975). These results have different constant factors which reflect the different convolution or filter functions used and the different models or parameterizations of the reconstructed density. Comparison with Radon inversion (Friedman, Beattie and Laughlin 1974) is difficult since resolution is not discussed.

4. Finite Number of Angles

When n_z is sufficiently large, but n_θ is of moderate size, multiplication by the matrix M remains a convolution (M_{kj} depends only on the relative coordinates of the j^{th} and k^{th} bins) but the convolution function is no longer the simple one given by $(d/\pi) < r_{kj}^{-1} >$ nor is it circularly symmetric. One may envision the convolution function by holding k constant and varying j. M_{kj} will have the familiar star or spoked pattern centered at cell k. Radially outward from the k^{th} cell (along the spokes) M_{kj} does not decrease when the distance between the j^{th} and k^{th} cells is greater than about $d/\Delta\theta$, where $\Delta\theta$ is the interval between angles.

In order to investigate the effect of a finite number of angles the matrix M (as calculated using eqn (A13) of the Appendix) has been inverted for n_θ = 8, 10, 12, 14, 16, 18, 20, 22, and 24 angles. The first angle is given by $\theta = \pi/2n_\theta$ in order to avoid $\theta = 0$ (fig. 1). Subsequent angles were generated by adding increments of π/n_θ. D/d for this inversion was 16 and total number of cells in the reconstruction was $\nu = 208$. In all cases the value of M_{jj} was very close to .95. (For large n_θ and n_z, $M_{jj} = .95$.) Fig. 2 shows the resulting average values of M_{jj}^{-1}, where the average has been taken over all cells except those at the very edge of the reconstruction region. As can be seen on fig. 2, $(M_{jj}^{-1})_{avg}$ decreases with increasing number of angles and approaches the value of 1.59 as expected. Note that the abscissa is labeled $n_\theta d/D$, and that no explicit reference is made to n_θ alone. It has been verified using D/d = 8, 24, and 32 that $(M_{jj}^{-1})_{avg}$ depends only on $n_\theta d/D$.

It can be seen from fig. 2 that when the number of angles reaches about 1.5 times the number of cells across the reconstruction region ($n_\theta d/D \simeq 1.5$) $(M_{jj}^{-1})_{avg}$ is very close to its limit of 1.59. For $n_\theta d/D = 1.0$, its value is already greater than 2.5 so that it is desirable to have $n_\theta d/D$ at least 1.0 and preferably 1.5 in order to make efficient use of the data. This is consis-

tent with the result of Klug and Crowther (1972) and Snyder and Cox (1975) which is that the number of angles required is given by $\pi D/(2d)$.

5. Finite Number of Line Integrals for each Angle

The average values of M_{jj}^{-1} have been computed for several values of n_θ and Δz, where Δz is the lateral spacing between line integrals at each angle. D/d was 16 and the averaging was performed over all cells except those at the edge of the reconstruction region. Angles were generated by the procedure given in the last section, and the lateral positions of the line integrals were chosen such that the center of the circular reconstruction region was halfway between two adjacent paths for each angle. In all cases the average value of M_{jj} was very close to .95. Fig. 3 shows $(M_{jj}^{-1})_{avg}$ for n_θ = 12, 16, 20, and 24 angles and values of Δz between zero and .85d.

For values of $\Delta z/d$ greater than .7, the individual values of M_{jj}^{-1} vary considerably from $(M_{jj}^{-1})_{avg}$. This is the effect of our model of square cells of uniform density and of the manner in which the paths for line integrals pass through the cells. The abscissa of fig. 3 is labeled $\Delta z/d$ with the assumption that the propagation of errors from the data to the reconstruction depends only on $n_\theta d/D$ (the number of angles divided by the number of cells across the reconstruction region) and the distance between line integrals relative to the cell size. Points for $\Delta z/d$ equal to zero have been taken from fig. 2.

As can be seen on fig. 3, $(M_{jj}^{-1})_{avg}$ increases rapidly for $\Delta z/d$ greater than 0.7, but is quite well behaved for $\Delta z/d$ less than 0.4. Thus, in order to obtain a reconstruction with resolution d, it is necessary to have the spacing between line integrals substantially less than d (.4d to .7d) in order to make efficient use of the data. This is in conflict with Synder and Cox (1975) where it is assumed that the resolution obtainable in a reconstruction is the same as the resolution in the projections.

The average variance of reconstructed cell densities based on the statistical uncertainty of the measurements, σ_I, can be calculated by averaging eqn (11) over cells in the reconstruction region,

$$(\sigma_\rho^2)_{avg} = \frac{D\sigma_I^2}{nd^3} (M_{jj}^{-1})_{avg} \tag{16}$$

Eqn (16) is applicable when there is a finite number of uniformly spaced angles, n_θ, and equally spaced line integrals for each angle, Δz, if values for $(M_{jj}^{-1})_{avg}$ are taken from fig. 3 for various combinations of n_θ and Δz.

6. Discussion

Eqn (11) expresses the expected variance of the least squares solution of eqn (1), the basic relationship between 2-dimensional density distribution and their line integrals. For an infinite number of data points, eqn (11) reduces to the simple expressions given by eqns (13) and (15). For a finite number of data points, eqn (16) expresses the expected average variance, where values for $(M_{jj}^{-1})_{avg}$ are taken from fig. 3 for various numbers of angles and lateral separation of line integrals.

It has been shown that for an infinite number of data points that the statistical fluctuations of the image are uniform over the reconstruction region. Evidence has been presented which supports the conclusion that the number of angles necessary to efficiently make use of the data is given by $\pi D/(2d)$, or about 1.5 times the number of cells across the reconstruction region. Finally, the lateral separation between line integrals should be substantially less than d, the linear cell dimension, preferably between .4d and .7d in order to limit statistical fluctuations in the image.

The single assumption made has been that the uncertainties of all measured line integrals are equal. This assumption is particularly appropriate for transverse section scans using monoenergetic heavy charged particles such as

protons or alpha particles. (Crowe et. al. 1975, Budinger et. al. 1975, Huesman, Rosenfeld and Solmitz 1975). This assumption is also a reasonable approximation for x-ray transmission scans of the human head when a water bath is used to partially equalize the fraction of x-rays transmitted

For x-ray transmission scanners which do not use a water bath, scans of the human head and chest are partially self-equalized. The bone at the periphery of the transverse sections tends to increase the attenuation of x-rays where the path length through the patient is shortest. For gamma ray emission scans it is expected that this work will provide a rough estimate of the expected statistical fluctuations of the reconstruction. In addition to the nonuniformity of measurement errors, the problem of attenuation has not been treated here.

The author gratefully acknowledges productive discussion with Dr. Thomas Budinger, Dr. Kenneth Crowe and Grant Gullberg. This work was supported in part by the ERDA and in part by the NIH.

APPENDIX

In this appendix it is shown that as n_θ and n_z ($n = n_\theta n_z$) become large, M_{kj} in eqn (4) approaches $(d/\pi) \langle r_{kj}^{-1} \rangle$, where $\langle r_{kj}^{-1} \rangle$ is the average inverse distance between points in the j^{th} and k^{th} cells. Eqn (4) is rewritten here for convenience.

$$M_{jk} = \frac{D}{nd^3} \sum_{i=1}^{n} \ell_{ik} \ell_{ij} \tag{4}$$

Let the function $E_k(x,y)$ be defined such that,

$$E_k(x,y) = \begin{cases} 1, \text{ if the point } (x,y) \text{ is in the } k^{th} \text{ cell} \\ 0, \text{ otherwise} \end{cases} \tag{A1}$$

then,

$$\ell_{ik} = \int d\ell' \, E_k(x',y') \tag{A2}$$

where the integral is carried out along the i^{th} path, so that

$$\begin{aligned} x' &= x'(\theta_i, z_i) = z_i \sin\theta_i + \ell' \cos\theta_i \\ y' &= y'(\theta_i, z_i) = z_i \cos\theta_i - \ell' \sin\theta_i \end{aligned} \tag{A3}$$

as shown on fig. 4. Similarly, ℓ_{ij} can be written as,

$$\ell_{ij} = \int d\ell'' \, E_j(x'', y'') \tag{A4}$$

where

$$\begin{aligned} x'' &= z_i \sin\theta_i + \ell'' \cos\theta_i \\ y'' &= z_i \cos\theta_i - \ell'' \sin\theta_i \end{aligned} \tag{A5}$$

and substitution of eqns (A2) and (A4) into eqn (4) gives

$$M_{kj} = \frac{D}{nd^3} \sum_{i=1}^{n} \int d\ell' \, E_k(x', y') \int d\ell'' \, E_j(x'', y'') \tag{A6}$$

The distance between paths for each angle is given by,

$$\Delta z = \frac{D}{n_z} \tag{A7}$$

and the interval between angles is given by

$$\Delta\theta = \frac{\pi}{n_\theta} \tag{A8}$$

and eqn (A6) can be rewriten as,

$$M_{kj} = \frac{\Delta\theta\Delta z}{\pi d^3} \sum_{i=1}^{n} \int d\ell' \, E_k(x', y') \int d\ell'' \, E_j(x'', y'') \tag{A9}$$

In the limit of large n_θ and n_z eqn (A9) becomes,

$$M_{kj} \xrightarrow[\substack{n_\theta \to \infty \\ n_z \to \infty}]{} \frac{1}{\pi d^3} \int d\theta dz d\ell' \, d\ell'' \, E_k(x', y') E_j(x'', y'') \tag{A10}$$

and by making the transformation of coordinates of eqns (A3) and (A5), eqn (A10) gives

$$M_{kj} \xrightarrow[\substack{n_\theta \to \infty \\ n_z \to \infty}]{} \frac{1}{\pi d^3} \int dx' dy' dx'' dy'' \, \frac{E_k(x', y') E_j(x'', y'')}{\sqrt{(x' - x'')^2 + (y' - y'')^2}} \tag{A11}$$

where the square root term in the denominator of eqn (A11) arises from the Jacobian of the transformation. The functions E_k and E_j in eqn (A11) limit the integrals to within the k^{th} and j^{th} cells respectively, and since the area of each cell is d^2, eqn (A11) may finally be rewritten as,

$$M_{kj} \xrightarrow[\substack{n_\theta \to \infty \\ n_z \to \infty}]{} \frac{d}{\pi} \langle r_{kj}^{-1} \rangle \tag{A12}$$

The integration of eqn (A10) is quite long and tedious, and the result is quoted here in two steps without proof:

$$M_{kj} \xrightarrow[n_z \to \infty]{} \sum_{i=1}^{n_\theta} \frac{\Delta\theta}{6\pi \sin^2\theta_i \cos^2\theta_i} \sum_{a=-1}^{1} \sum_{b=-1}^{1} (-2)^{(2-|a|-|b|)} \tag{A13}$$

$$(Y \cos\theta_i - X \sin\theta_i)^3 \, H \, (Y \cos\theta_i - X \sin\theta_i)$$

$$M_{kj} \xrightarrow[\substack{n_\theta \to \infty \\ n_z \to \infty}]{} \frac{1}{12\pi} \sum_{a=-1}^{1} \sum_{b=-1}^{1} (-2)^{(2-|a|-|b|)} \left[3X^2Y \ln \frac{R+Y}{R-Y} + 3XY^2 \ln \frac{R+X}{R-X} - 2R^3 \right] \tag{A14}$$

where

$$H(q) = \begin{cases} 1, \text{for } q > 0 \\ 0, \text{for } q < 0 \end{cases} \tag{A15}$$

$$X = x + a$$

$$Y = y + b$$

$$R = \sqrt{X^2 + Y^2} = \sqrt{(x + a)^2 + (y + b)^2}$$

and x and y are the lateral displacements between the k^{th} and j^{th} cells in and x and y directions respectively measured in unites of d. For x = y = 0 in eqns (A14) and (A15) the result is,

$$M_{jj} \xrightarrow[\substack{n_\theta \to \infty \\ n_z \to \infty}]{} \frac{4}{3\pi} [3 \ln(\sqrt{2} + 1) - (\sqrt{2} - 1)] = .95 \tag{A16}$$

REFERENCES

BARRETT, H.H., BOWEN, T., HERSHEL, R.S., GORDON, S.K., and DELISE, D.A., 1975, in Technical Digest of Image Processing for 2-D and 3-D Reconstruction from Projections: Theory and Practice in Medicine and the Physical Sciences, Stanford, California 4-7 August 1975.

BUDINGER, T.F., CROWE, K.M., CAHOON, J.L., ELISCHER, V.P., HUESMAN, R.H., KANSTEIN, L.L., 1975, in Technical Digest of Image Processing for 2-D and 3-D Reconstruction from Projections: Theory and Practice in Medicine and the Physical Sciences, Stanford, California, 4-7 August 1975.

BUDINGER, T.F. and GULLBERG, G.T., 1974, IEEE Trans, Nucl. Sci., NS-21 (3), 2.

CHESLER, D.A., 1975, in Proceedings of the Workshop of Reconstructive Tomography in Diagnostic Radiology and Nuclear Medicine, San Juan, Puerto Rico, April 17-19, 1975.

CROWE, K.M., BUDINGER, T.F., CAHOON, J.L., ELISCHER, V.P., HUESMAN, R.H., and KANSTEIN, L.L., 1975, in Technical Digest of Image Processing for 2-D and 3-D Reconstruction from Projections: Theory and Practice in Medicine and the Physical Sciences, Stanford, California, 4-7 August 1975.

FRIEDMAN, M.I., BEATTIE, J.W., and LAUGHLIN, J.S., 1974, Phys. Med. Biol, 19, 819.

GOITEIN, M., 1972, Nuc. Inst. and Meth., 101, 509.

GORDON, R. and HERMAN, G.T., 1973, Int. Rev. Cytol., 38, 111.

HUESMAN, R.H., 1975, Lawrence Berkeley Laboratory Report LBL-4278.

HUESMAN, R.H., ROSENFELD, A.H. and SOLMITZ, F.T., 1975, Lawrence Berkeley Laboratory Report LBL-3040.

KLUG, A. and CROWTHER, R.A., 1972, Nature, Lond. 238, 435.

SHEPP, L.A. and LOGAN, B.F., 1974, IEEE Trans. Nucl. Sci., NS-21, (3), 21.

SNYDER, D.L. and Cox, J.R., 1975, Proceeding of the Workshop on Reconstructive Tomography in Diagnostic Radiology and Nuclear Medicine, San Juan, Puerto Rico, April 17-19, 1975.

TANAKA, E. and IINUMA, 1975, Phys. Med. Biol, 20, 789.

Figure Captions

Fig. 1. Geometry of the reconstruction region and an example of line integral paths at one angle, θ.

Fig. 2. Average value of the diagonal elements of the inverse of the matrix M as a function of the number of projection angles divided by the number of cells across the reconstruction region. Infinitesimal lateral spacing of line integrals is assumed.

Fig. 3. Average value of the diagonal elements of the inverse of the matrix M as a function of the number of projection angles divided by the number of cells across the reconstruction region and the lateral spacing of line integrals divided by the linear dimension of a cell.

Fig. 4. Geometry for the transformation from the $(\theta, z, \ell', \ell'')$ coordinate system to the (x', y', x'', y'') coordinates system.

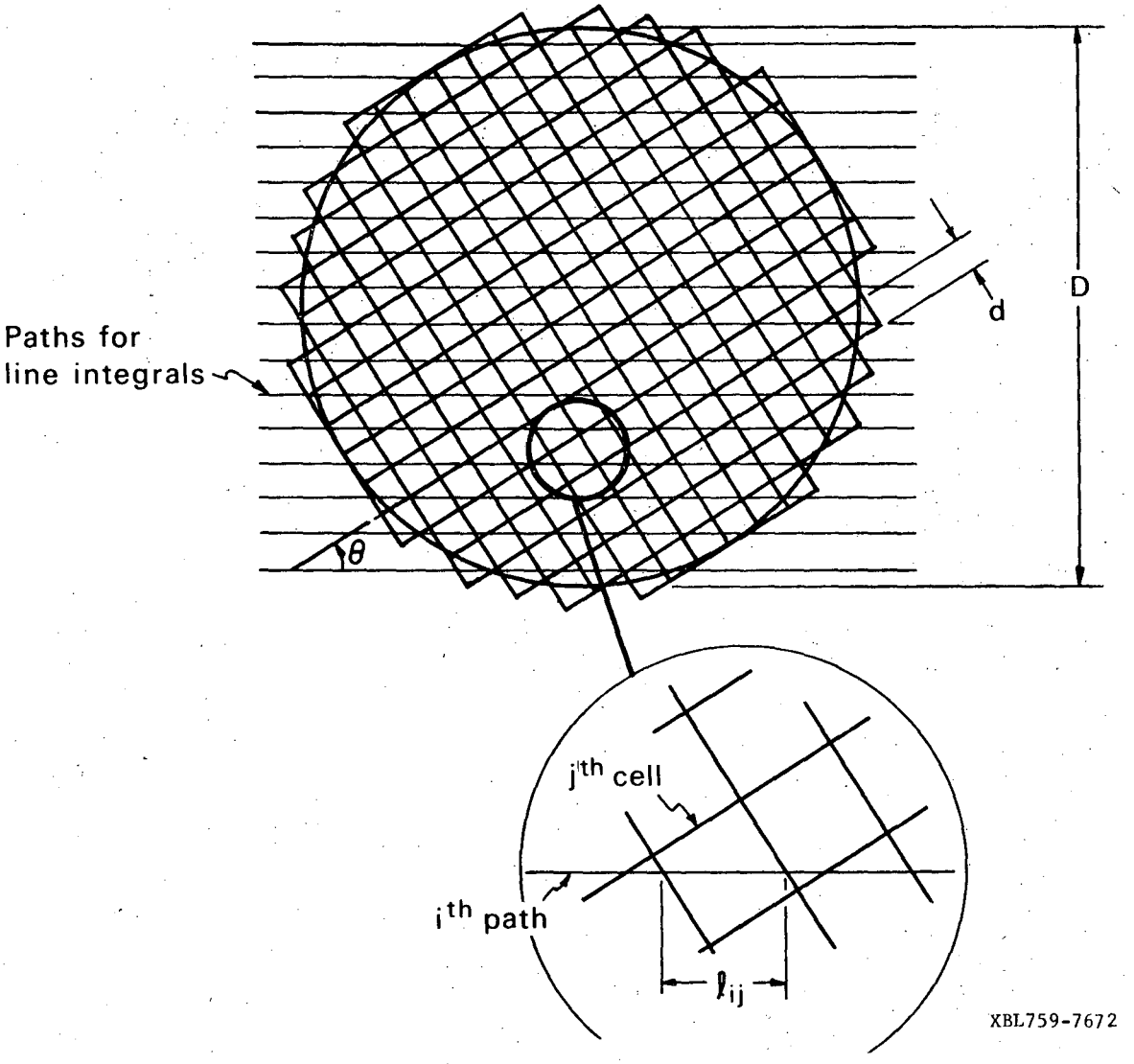

FIG. 1.

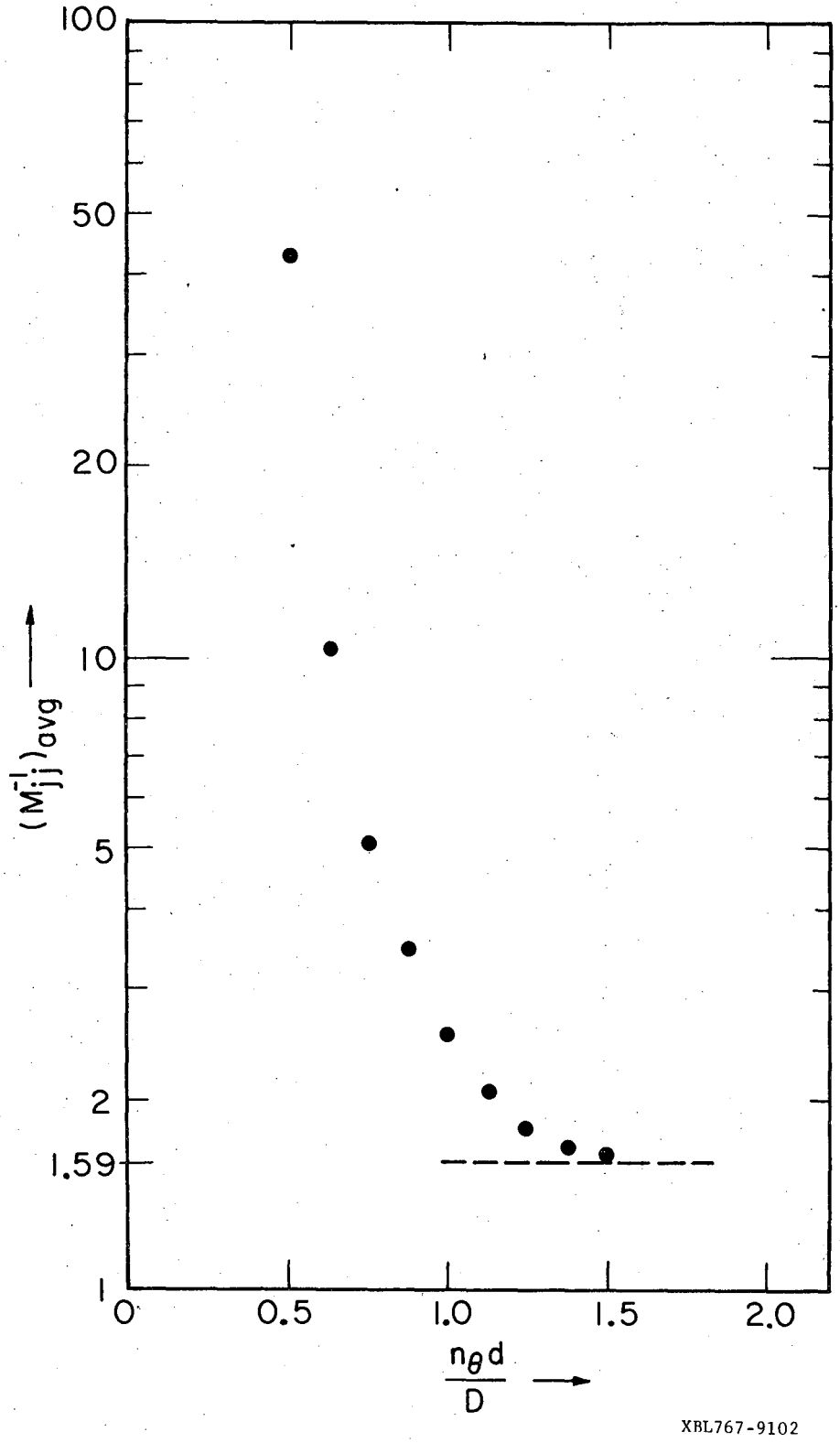
100
50
20
10
5
2
1.59
1
0
0.5
1.0
1.5
2.0
$(M_{jj}^{-1})_{avg}$
$\frac{n_\theta d}{D}$
XBL767-9102

FIG. 2

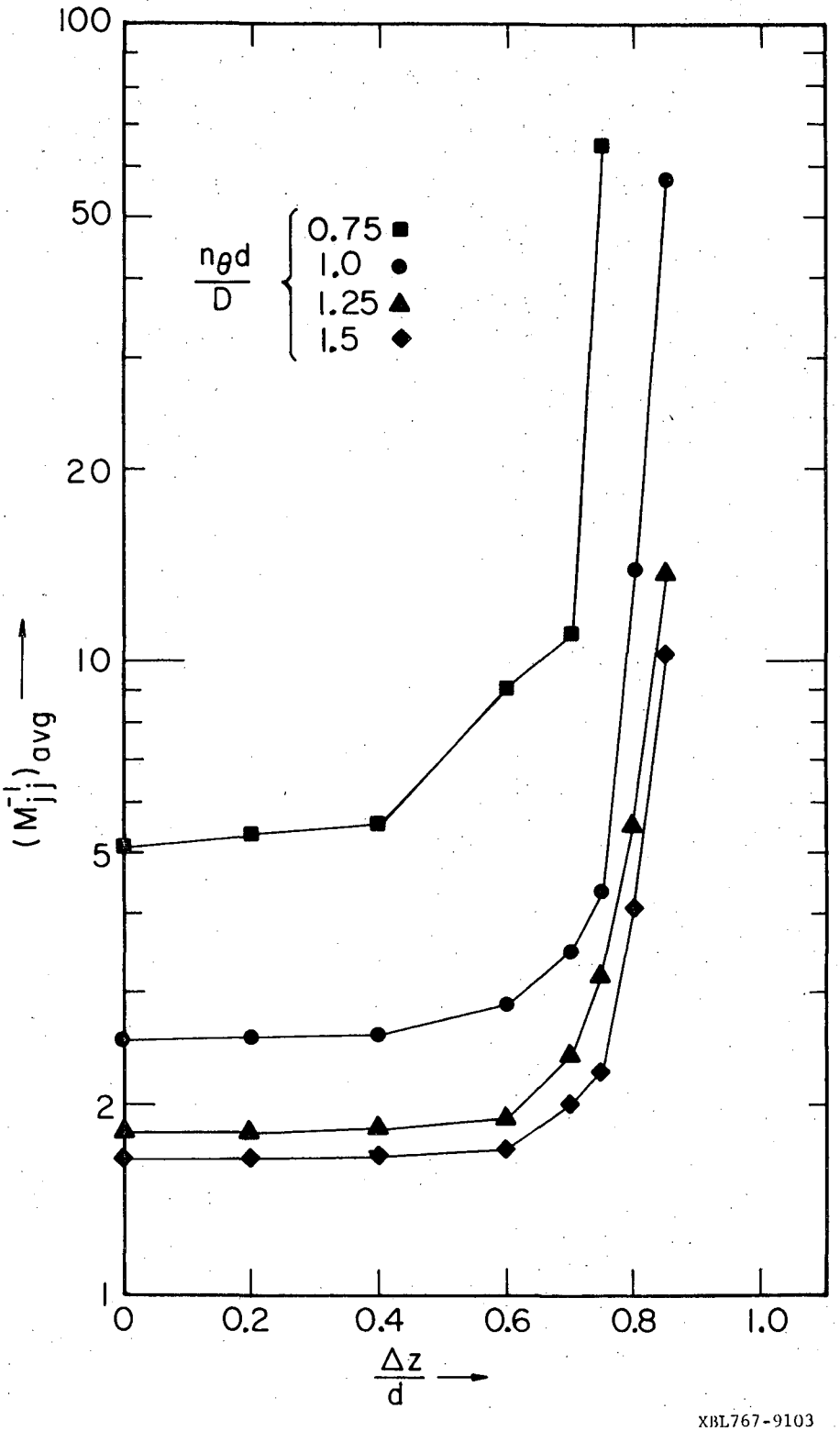
100
50
20
10
5
2
1
0
0.2
0.4
0.6
0.8
1.0
$\frac{n_\theta d}{D}$
0.75
1.0
1.25
1.5
$(M_{jj}^{-1})_{avg}$
$\frac{\Delta z}{d}$
XBL767-9103

FIG. 3

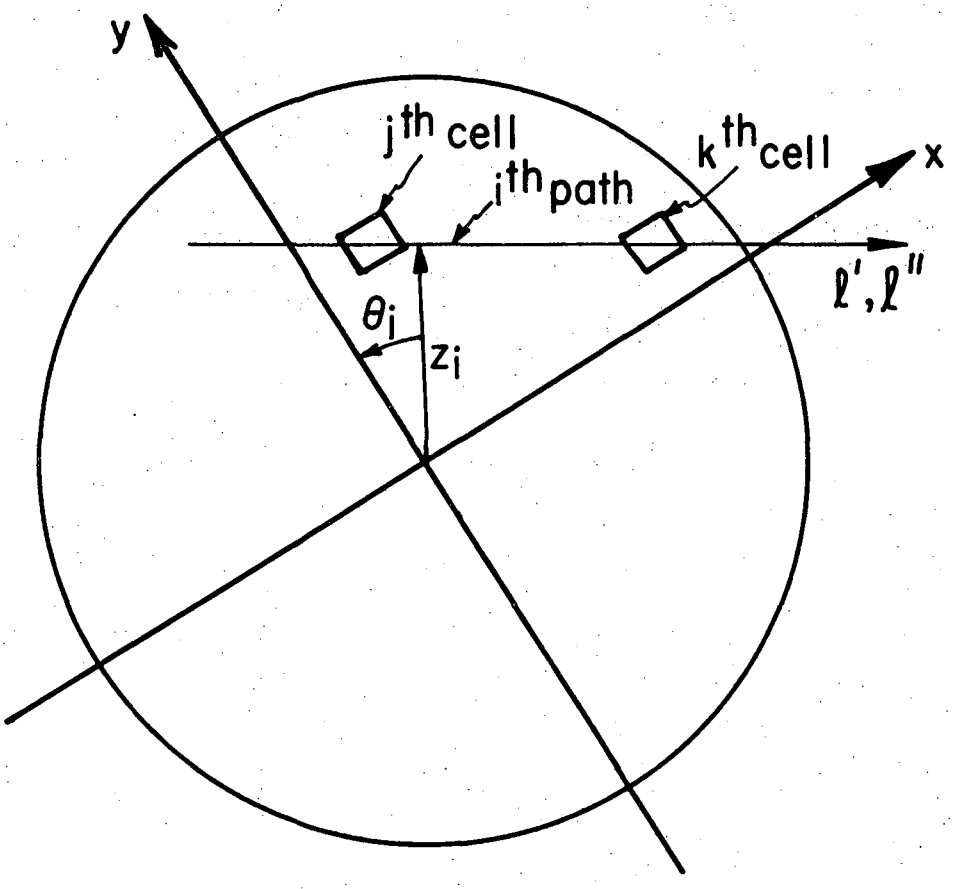

XBL764-5441

FIG. 4

TECHNICAL INFORMATION DIVISION
LAWRENCE BERKELEY LABORATORY
UNIVERSITY OF CALIFORNIA
BERKELEY, CALIFORNIA 94720